CrossMark
click for updates

Influence of negative-*U* centers related carrier dynamics on donor-acceptor-pair emission in fluorescent SiC

Yi Wei, Abebe Tilahun Tarekegne, and Haiyan Ou[a)]
Department of Photonics Engineering, Technical University of Denmark, DK-2800 Kgs. Lyngby, Denmark

E_1/E_2 defects are the typical negative-*U* centers in *n*-type 6H silicon carbide (SiC). They are the main contributors to non-radiative recombination, which limits the carrier lifetime. In this study, two fluorescent 6H silicon carbide (f-SiC) samples and one bulk substrate were characterized via time-resolved photoluminescence (TRPL) and static photoluminescence (PL) measurements, where all the samples were nitrogen-boron co-doped 6H *n*-type. The existence of E_1/E_2 defects, which caused the diminution of the internal quantum efficiency (IQE) and luminescence intensity of each sample, was confirmed by applying a carrier dynamics model based on negative-*U* centers. The carrier dynamics simulation reveals that the density of the E_1/E_2 defects in bulk 6H SiC is two orders of magnitude higher than that of the f-SiC sample, causing much lower PL intensity in the bulk substrate compared to the two f-SiC samples. The IQE of the two f-SiC samples was extracted from the corresponding TRPL results, where the contrast between their IQE was further confirmed by the related PL measurement results. The slight difference in IQE between the two f-SiC samples was attributed to slightly different E_1/E_2 defect concentrations. On the other hand, by implementing a steady-state donor-acceptor-pair (DAP) recombination calculation, it was found that the f-SiC sample with lower IQE had a higher DAP transition probability due to the higher doping level. This prompted further optimizations in the f-SiC crystal growth conditions in order to decrease the E_1/E_2 defects while maintaining the correct doping parameters. *Published by AIP Publishing.*
https://doi.org/10.1063/1.5037167

I. INTRODUCTION

Fluorescent silicon carbide (f-SiC) is a novel optoelectronic material capable of displaying strong orange-yellow light emission with a broad spectrum.[1] Owing to its sufficient thickness ($>10 \mu m$) with high-density ($>10^{18}$ cm^{-3}) donor-acceptor-pairs (DAPs),[1] f-SiC is anticipated to realize efficient wavelength conversion from the near-ultraviolet (NUV) to the visible light spectral region. The high density of DAP is achieved by the heavy nitrogen (N) and boron (B) co-doping during growth where *n*-type f-SiC is eventually formed. f-SiC has a number of properties amenable to future requirements for solid-state lighting. For instance, compared with yellow phosphors, f-SiC contains no rare-earth elements[2] and has no issue of degradation; hence, it is believed that[1–5] f-SiC is a promising substitute for yellow phosphors for future white light-emitting diodes (LEDs). Besides, its high thermal conductivity makes it ideal for high power LED applications. Much progress has been made toward realizing the new type of white LEDs based on f-SiC. For instance, a prototype of white LED was proposed through f-SiC being pumped by a gallium nitride (GaN) based multiple-quantum-well (MQW) NUV source,[2,4] where the NUV stack was grown on the f-SiC substrate. Meanwhile, efforts have also been made toward enhancing the light extraction efficiency of f-SiC by using, e.g., antireflective subwavelength conical[6] and wavelength-scale nanodome structures,[7] which have resulted in enhancements of 66.3% and 138%, respectively. Later on, the hybrid f-SiC structure combining

as-grown f-SiC with the porous f-SiC surface layer[8] has achieved white light emission with a color rendering index (CRI) as high as 81.1. As the luminescence efficiency is the cornerstone of the lighting source based on f-SiC where the emission quality is quite sensitive to the doping levels of both *n*- and *p*-type dopants, a lot of efforts have been made toward optimizing the doping conditions. It has been found that both B and N concentrations are required to exceed 10^{18} cm^{-3} and the difference between those two concentrations needs to be larger than 4×10^{18} cm^{-3} (Refs. 9 and 10) in order to induce high intensity DAP recombination.

However, the internal quantum efficiency (IQE) of typical f-SiC samples is still fairly low, indicating that a significant proportion of carriers goes through non-radiative recombination pathways. Several studies have been reported about the investigations on the non-radiative recombinations in f-SiC through experimental approaches. It was first found that[5] the centers for non-radiative recombinations are distinct from the DAP recombination centers in f-SiC. Later on, it was suggested that[11] the competing recombination regime against DAP recombination in f-SiC might be related to E_1/E_2 centers. Likewise, it was also believed that[12] the nitrogen doping could facilitate the formation of the vacancy related defects, e.g., the E_1/E_2 centers which contribute to non-radiative recombinations. In fact, the E_1/E_2 centers have been identified as the dominating intrinsic point defects in *n*-type 6H SiC[13–15] and found to originate from the same point defects as the Z_1/Z_2 centers in 4H SiC.[16,17] It is widely accepted that the E_1/E_2 centers are related to the carbon vacancy (V_C) in 6H SiC.[13,15,18]

[a)]Electronic mail: haou@fotonik.dtu.dk

By characterizing an n-type 6H SiC-based Schottky diode via deep level transient spectroscopy (DLTS), it was discovered that[19] E_1/E_2 centers were associated with two acceptor-like levels and might be important for electron-hole (e^--h^+) pair recombination. Soon afterwards, the DLTS peaks of E_1/E_2 centers were found[20] to correlate with a two-stage ionization process from either the E_1^- or E_2^- acceptor levels, where the charge states of either center was transferred in the sequence $E_{1/2}^- \rightarrow E_{1/2}^0 + e^- \rightarrow E_{1/2}^+ + 2e^-$ ($E_{1/2}$ represents the E_1 or E_2 center) associated with single e^- emission within each stage. This two-stage ionization indicated that the binding energies of E_1/E_2 centers were strengthened when capturing the second e^-, suggesting the existence of the so-called negative-U system.[21] Assuming that two e^- are bound to a lattice-vacancy in a group-IV semiconductor,[22] one e^- should normally be bound more tightly to the defect if the other e^- has been removed. However, if the ionization of the e^- which was captured by the defect later requires larger energy, the related defect center is said to possess a negative-U property. As these two e^- are being paired in the dangling bonds of a defect and meanwhile being coupled with a large lattice relaxation,[23] it could give rise to considerable energy gain for the e^- pairs. The cause of this negative-U behavior, where two e^- appear to have a net attractive interaction macroscopically, could be explained by the fact that the energy gain of e^- is able to break the Coulomb barrier between the two e^-. A theoretical framework[24,25] via *first-principles* calculations has been developed to study the negative-U behavior of the carbon vacancy in SiC. It was found that the generation of a carbon vacancy in SiC is accompanied by significant Jahn-Teller distortion, where the aforementioned energy gain of an e^- is actually introduced by the Jahn-Teller distortion in the case of neutral carbon vacancy with a symmetry lowering.

Although E_1/E_2 centers have been widely observed by applying DLTS on as-grown and irradiated 6H SiC samples,[13–15,17–19,26,27] so far, the DLTS measurement report is not available for f-SiC samples. It is still difficult to fabricate a metal-insulator-semiconductor (MIS) structure Schottky diode with low leakage current based on f-SiC for DLTS measurements because of the very high free carrier density at thermal equilibrium.[28,29] Alternatively, in order to study how E_1/E_2 centers affect the IQE of f-SiC which is mainly dependent on the radiative DAP recombination, it is preferable to apply time-resolved photoluminescence (TRPL) and static photoluminescence (PL) measurements on f-SiC, since they are nondestructive methods and do not require time-intensive contact preparation.

In this work, we quantitatively demonstrate how the negative-U centers (E_1/E_2 defects) affect recombination in f-SiC in parallel with the DAP recombination process. The rapid luminescence decay in f-SiC is successfully explained by applying a negative-U center related carrier dynamics model. A steady-state DAP recombination model is also implemented to reveal how the DAP related process could be affected by the presence of negative-U centers. Moreover, we investigated the carrier dynamics of N-B co-doped n-type 6H bulk SiC to compare with f-SiC and showed that an

additional trapping center is found other than E_1/E_2 defects in the bulk material.

II. EXPERIMENTAL

TRPL measurements of 6H SiC were previously done by others to extract information about different recombination channels which could be either radiative or non-radiative.[30,31] Here, we believe that two recombination channels corresponding to negative-U centers assisted recombination and DAP recombination are present. By applying the multi-phase exponential decay fitting to the measured TRPL curves, two parameters of each recombination channel can be obtained: the recombination lifetime (time constant) and the amplitude which indicates the relative "load capacity" of the non-equilibrium carriers. On the other hand, the static PL characterizations were applied in order to get the relative efficiency of the steady-state DAP recombination. Based on the parameters extracted from each recombination channel, the reason for the different static PL intensities measured for different samples were interpreted quantitatively. The related computational methods will be introduced in Sec. III.

The specifications of the three samples employed in this research, labelled as EP-A, EP-B ("EP" for the f-SiC epilayer), and BK ("BK" represents the 6H bulk SiC), are summarized in Table I. The epilayers of the f-SiC samples were grown on the $(000\bar{1})$ plane with low off-axis (orientation: $\langle 11\bar{2}0 \rangle \pm 1.4°$) and $250\,\mu m$ thick 6H SiC substrates (SiCrystal GmbH) using the fast sublimation growth process (FSGP)[32,33] at $1725\,°C$. A commercial (TanKeBlue Ltd.) 6H bulk SiC sample with top and bottom sides (orientation: $\langle 0001 \rangle \pm 0.5°$) polished using chemical mechanical polishing (CMP) was applied as the reference.

Both TRPL and PL measurements were performed at room temperature (RT). Both the input laser beam and the emission signal to be detected were fiber-coupled to a $50\times$ microscope lens in a front excitation/front detection

TABLE I. Essential parameters of each 6H SiC sample.

Sample ⇒	EP-A	EP-B	BK
d (μm)[a]	45 + 250		325
Dim. (cm^2)	0.8×0.5	1.2×1.2	0.5×0.5
N_d ($\times 10^{18}$ cm^{-3})[b]	9.0	9.2	5.4
N_a ($\times 10^{18}$ cm^{-3})[b]	4.4	5.2	0.95
E_g (meV)[c]	2984	2982	2998
E_F (meV)[c]	2885	2879	2903
n_0 ($\times 10^{18}$ cm^{-3})[c]	1.90	1.69	2.34
N_u ($\times 10^{12}$ cm^{-3})[d]	2.08	3.50	172
Z_{eff} (μm)[e]	17.33		
g (cm^{-3})[e]	4.57×10^{11}		

[a]The sample thickness (d) for f-SiC samples is the sum of the epilayer and the substrate.
[b]The dopant concentrations (Nitrogen: N_d | Boron: N_a) were characterized by secondary-ion mass spectroscopy (SIMS).
[c]The calculation of the bandgap (E_g), the Fermi level (E_F), and the carrier density at thermal equilibrium (n_0) is derived from Refs. 36 and 72–75.
[d]The determination of the total density of the negative-U center (N_u) of each sample can be found in Sec. III A.
[e]The effective penetration depth (Z_{eff}) and the injection level (g) were determined by the methods mentioned in Sec. II.

configuration. For either TRPL or PL measurement, different numbers of spots were characterized on different samples (BK: two/EP-A: three/EP-B: nine) considering the dimension of each sample shown in Table I.

The key components of the experimental setup of the TRPL system were from PicoQuant GmbH. Short laser pulses were generated by a picosecond diode laser (LDH828, $\lambda = 375$ nm, 44 ps pulse width with a pulse repetition rate up to 80 MHz). The laser beam was focused onto the sample via the $50\times$ lens with a numerical aperture (NA) of 0.8, where the diameter (D) of the laser spot on the sample was measured to be approximately 0.22 mm. After that, the emitted photons from the sample were filtered by a long-pass 405 nm filter and then detected by a photon-multiplier tube (PMA Hybrid). Finally, the photoluminescence decay was recorded by a time correlated single photon counting system (abbrev. TCSPC, TimeHarp 260 NANO).

The criterion for choosing the time span for each measurement was to record the decay profile as complete as possible while preventing interference from the background noise [typically 80–120 counts per second (cps)]. 20 μs/2 ms ranges were chosen for sample BK/sample EP-A(B), respectively. A 500 Hz repetition rate laser pulse was chosen for the measurement on the two f-SiC samples with a resolution of 80 ns and an integration time of 1 h. Accordingly, the 50 kHz laser pulse with a beam power of $\sim$91.35 nW was chosen for the measurement of the bulk sample with a ps resolution of 800 and an integration time of 30 min for the more rapid decay. In order to calculate the injection level g (cm^{-3}) which is essential for our modelling, the pulsed beam power was measured by an optical power meter (Thorlabs PM100D). Here, we believed that the energy of a single pulse is independent of the pulse repetition rate; hence, we measured the beam power at a repetition rate of 500 kHz to eliminate the interference from noise and obtained a beam power of $\sim$920 nW. We implemented this value to the calculations of the injection levels for all three samples. Then, we calculated the photon density I_0 (cm^{-2}) of the laser spot. The average injection level was determined by assuming an effective depth[34] $Z_{eff} = \alpha^{-1} \ln[2/(1 + e^{-\alpha d})]$, where α (cm^{-1}) is the absorption coefficient of 6H SiC and d is the layer thickness of the sample. Here, the absorption coefficient of 6H SiC with polarization of the laser source oriented perpendicular to the c-axis ($\mathbf{E}\perp\mathbf{c}$) at 375 nm (Ref. 35) is about 400 cm^{-1}. Then, the injection level, which is dependent on Z_{eff}, can be given by $g = \alpha \times I_0 \times e^{-\alpha Z_{eff}}$. Z_{eff} and the corresponding g were calculated to be almost independent of sample thickness d and fixed at $17.33\,\mu$m $|\,4.57 \times 10^{11}$ cm^{-3}, respectively, for all three samples.

For PL measurements, the same pulsed laser source was applied where the pulse repetition rate was set to 500 kHz with a beam power of $\sim$920 nW. This was to make sure that the PL intensities were measured under the same condition as the TRPL, where the injection level per pulse for PL measurements was set to be identical to that of the TRPL measurements. An optical spectrometer (CAS 140B, Instrument Systems GmbH) was implemented with the integration time set to 5 s for all PL measurements. The emitting photons from the frontside of the sample were filtered by a long-pass filter ($\lambda_{cutoff} = 420$ nm).

III. COMPUTATIONAL METHODS

In order to understand why the PL intensities of the three 6H SiC samples differ, the competitive relation between the negative-U centers assisted recombination and the DAP recombination needs to be analyzed numerically. This could be achieved by combining the negative-U center related carrier dynamics and the steady-state DAP recombination calculation together, where the parameters of the corresponding recombination channels are applied for the inputs of each in the model.

The overall framework of the negative-U center related carrier dynamics simulation was based on the method used in Ref. 34. The authors discussed the carrier dynamics simulation of the negative-U centers Z_1/Z_2 in 4H SiC, where the Z_1 and Z_2 centers were combined together as a single negative-U center in the simulation. Since the equivalence between the Z_1/Z_2 centers in n-type 4H SiC and the E_1/E_2 centers in n-type 6H SiC has been confirmed by previous research,[15,37] the methodology is also applicable for modelling the E_1/E_2 center related carrier dynamics in 6H SiC. Nevertheless, substantial changes have been made in this calculation, e.g., the carrier dynamics related to the three types of negative-U centers (introduced in Sec. III A) in 6H SiC were simulated separately. In addition, the influence of the heavy boron doping on the carrier dynamics was also taken into consideration. The details about the carrier dynamics simulation in 6H SiC will be further illustrated in Sec. III A.

The approach for the calculation of the DAP recombination lifetime (τ_{dap}) was adopted from Ref. 38, where the authors describe a steady-state model for single DAP recombination in semiconductors. The model was applied for each DAP recombination channel in 6H SiC where three donor levels and one acceptor level were included. The DAP transition probability $W(r_{dap})$ is the crucial parameter for calculating τ_{dap}. In this work, we quantitatively demonstrate how the mean DAP separation distance r_{dap} influences $W(r_{dap})$ and how $W(r_{dap})$ further affects τ_{dap}. In addition, the estimations for the capture probabilities of each donor and acceptor are discussed. The details about the calculation of the DAP recombination lifetime in 6H SiC will be further illustrated in Sec. III B.

Suttrop et al.[39] observed yellow luminescence with λ_{peak} = 580 nm from the nitrogen-boron co-doped 6H SiC epilayer, where they attributed this luminescence to the phonon replica of the DAP recombination related to the boron-induced deep center (D-center) located at 0.58 eV above the valence band. In our experiment, the orange-yellow emissions were observed in the three samples with λ_{peak} around 580 nm. Hence, in either the negative-U center related carrier dynamics simulation or the τ_{dap} calculation, the D-center was the only acceptor level in 6H SiC taken into consideration. The general parameters of nitrogen/boron co-doped n-type 6H SiC applied in this work are listed in Table II.

A. Carrier dynamics related to negative-U centers

Based on the previous results[19,20] about the characterization of E_1/E_2 centers in 6H SiC via the DLTS technique, the more recent findings by Koizumi et al.[42] have revealed that the E_2 center could be further separated into two centers E_{2L} and E_{2H}. The subscripts "L" and "H" indicate that the DLTS

TABLE II. General characteristics of the nitrogen/boron co-doped n-type 6H SiC.

Parameter	Symbol	Value	References
e^- effective mass	m_e^*	$0.71m_0$ [a]	40
h^+ effective mass	m_h^*	$0.90m_0$ [a]	40
Binding energy of			
Donor level (cubic site c_1)	ΔE_{c1}	137.6 meV	41
Donor level (cubic site c_2)	ΔE_{c2}	142.4 meV	41
Donor level (hexagonal site h)	ΔE_h	81 meV	41
Acceptor level (D-center)	ΔE_D	580 meV	39
Activation energy of the charge state:			
E_1^-	$\Delta E_1^{0/-}$	390 meV	42
E_{2L}^-	$\Delta E_{2L}^{0/-}$	440 meV	42
E_{2H}^-	$\Delta E_{2H}^{0/-}$	430 meV	42
E_1^0	$\Delta E_1^{+/0}$	260 meV	42
E_{2L}^0	$\Delta E_{2L}^{+/0}$	140 meV	42
E_{2H}^0	$\Delta E_{2H}^{+/0}$	180 meV	42
Thermal barrier of:			
$E_1^0 + e^- \rightarrow E_1^-$ transition	ε_{b1}	48 meV	20
$E_2^0 + e^- \rightarrow E_2^-$ transition	ε_{b2}	70 meV	20
e^- capture cross section of:			
$E_1^0 + e^- \rightarrow E_1^-$ transition	$\sigma_{1,e}^{0/-}$ [b]	3×10^{-15} $\times \exp\left(-\varepsilon_{b1}/(k_b T)\right)$ cm^{-2}	20 and 42
$E_1^+ + e^- \rightarrow E_1^0$ transition	$\sigma_{1,e}^{+/0}$	2×10^{-15} cm^{-2}	42
$E_{2L}^0 + e^- \rightarrow E_{2L}^-$ transition	$\sigma_{2L,e}^{0/-}$ [b]	6×10^{-15} $\times \exp\left(-\varepsilon_{b2}/(k_b T)\right)$ cm^{-2}	20 and 42
$E_{2L}^+ + e^- \rightarrow E_{2L}^0$ transition	$\sigma_{2L,e}^{+/0}$	5×10^{-16} cm^{-2}	42
$E_{2H}^0 + e^- \rightarrow E_{2H}^-$ transition	$\sigma_{2H,e}^{0/-}$ [b]	5×10^{-15} $\times \exp\left(-\varepsilon_{b2}/(k_b T)\right)$ cm^{-2}	20 and 42
$E_{2H}^+ + e^- \rightarrow E_{2H}^0$ transition	$\sigma_{2H,e}^{+/0}$	7×10^{-16} cm^{-2}	42

[a]m_0 refers to the free electron mass.
[b]k_b refers to the Boltzmann constant.

peak of E_{2L} emerged at a lower emission rate, whereas the DLTS peak of E_{2H} emerged at a higher emission rate at certain temperatures. All three negative-U centers are classified as carbon vacancy-related centers[15] where E_1 defects are located at the hexagonal sites while E_{2L} and E_{2H} defects are located at the cubic sites[13] in 6H SiC. In this investigation, the negative-U center related carrier dynamics is based on the above-mentioned three non-equivalent defect centers.

The schematic band diagram of the non-equilibrium carrier capture process related to the negative-U centers in 6H SiC is shown in Fig. 1. At RT, the E_i^- state acts as the ground state, where the subscript "i" ($i \Rightarrow 1$, $2L$, and $2H$) designates the component of the negative-U system. This means that after the transient interaction between the injected non-equilibrium carriers and the sample material, all the excited charge states E_i^0 and E_i^+ would return ideally back to the E_i^- state. Note that the carrier emission from each charge state is negligible at RT[34] due to very large activation energies; therefore, only the carriers' capture was considered in this simulation. Since all three samples have fairly high densities of the boron dopant ($>10^{17}$ cm^{-3}), the influence of the acceptor level (D-center) on the carrier dynamics cannot be negligible, where all the non-equilibrium h^+ occupy the acceptor level and almost impossible to be ionized into the valence band due to the large ionization energy.[9] Therefore, the negative-U center related h^+ capture is believed to come from the D-center rather than the valence band in this

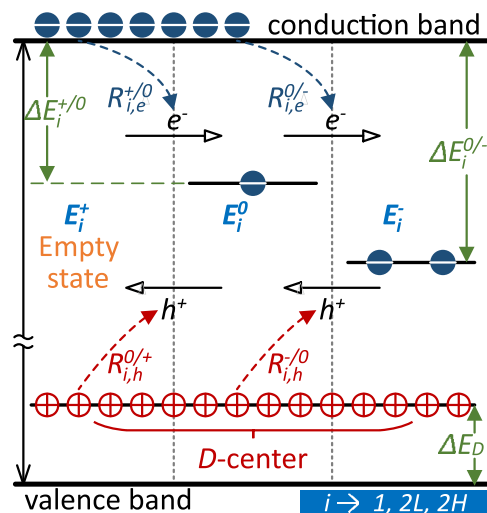

FIG. 1. A schematic band diagram of the capture process of non-equilibrium carriers via the negative-U center in 6H SiC at RT. The subscript "i" suggests the component of the negative-U system: E_1, E_{2L}, or E_{2H}, each of which consists of three charge states ($E_i^+/E_i^0/E_i^-$) separated by the gray dashed lines. The capture of e^- from the conduction band or h^+ from the D-center, which is marked by the dashed arrow, is involved in the transitions of either $E_i^+ \rightleftharpoons E_i^0$ or $E_i^0 \rightleftharpoons E_i^-$ which are labelled with the open arrows. The activation energy of the shallow-donor-like E^0 state or the acceptor-like E^- state is indicated by $\Delta E_i^{+/0}$ or $\Delta E_i^{0/-}$, respectively, whereas the binding energy of the D-center is indicated by ΔE_D.

condition. The e^- capture involved in the transition from the empty state (E_i^+) to the intermediate state (E_i^0) is considered as a fast cascaded capturing process,[43,44] while the transition from the E_i^0 to the E_i^- involving the e^- capture is considered as the slow multiphonon process[20] in which the transition energy for e^- capture must be corrected with the thermal barrier. The corresponding thermal barrier for defects on hexagonal (E_1) and cubic (E_2) sites and the corrected $\sigma_{i,e}^{0/-}$ for three centers are given in Table II.

It was believed that[19] the capture rate of h^+ should be in the same order or higher than that of the e^- for one negative-U center. Later on, a more specific relation where $\sigma_{i,h}^{-/0} \approx \sigma_{i,h}^{0/+} \approx (5 \sim 10) \times \sigma_{i,e}^{+/0} \gg \sigma_{i,e}^{0/-}$ was reported.[34] By fixing the value of $\sigma_{i,h}^{-/0}(\sigma_{i,h}^{0/+})$, the density of the negative-U center can be estimated once the negative-U center related minority carrier lifetimes $\tau_{u,i}$ at a low injection level are measured.[45] Here, we assume $\sigma_{i,h}^{-/0}, \sigma_{i,h}^{0/+} = \sigma_{i,h}$, and the expression of the density of each negative-U center $N_{u,i}$ in 6H SiC is shown in Eq. (1), where $\langle \nu_{th,h} \rangle$ represents the mean thermal velocity of h^+ (see Appendix A). Hereon, we assumed the relation $\sigma_{i,h}^{-/0} = \sigma_{i,h}^{0/+} = 5 \times \sigma_{i,e}^{+/0}$ in the carrier dynamics simulation for simplicity.[46]

The general conditions of negative-U center related carrier dynamics are formulated in Appendix A. In particular, for the case of low injection level plus high carrier density in the three 6H SiC samples (see Table I), one can suggest that $n_0 \gg \delta n_i(t)$, $p_0 \ll \delta p_i(t)$, and $\delta p_i(t) \gg p_i^{0/+}, p_i^{-/0}$. By further applying Eqs. (A2) and (A3) into Eq. (A1), the carrier capture rates can be rewritten in an analytical form as shown below

$$N_{u,i} = \frac{1}{\sigma_{i,h}\langle \nu_{th,h}\rangle \tau_{u,i}}, \tag{1}$$

$$R_{i,e}^{0/-}(t) = \sigma_{i,e}^{0/-}\langle \nu_{th,e}\rangle \Big\{ n_0\big[\delta p_i(t) - \delta n_i(t) - 2\delta N_i^-(t)\big]$$
$$-n_i^{0/-}\big[N_{u,i} + \delta N_i^-(t)\big]\Big\}, \tag{2a}$$

$$R_{i,e}^{+/0}(t) = \sigma_{i,e}^{+/0}\langle \nu_{th,e}\rangle \Big\{ (n_0 + n_i^{+/0})[\delta n_i(t) - \delta p_i(t)]$$
$$+(n_0 + 2n_i^{+/0})\delta N_i^-(t)\Big\}, \tag{2b}$$

$$R_{i,h}^{-/0}(t) = \sigma_{i,h}^{-/0}\langle \nu_{th,h}\rangle \Big\{ \delta p_i(t)\big[N_{u,i} + \delta N_i^-(t)\big]\Big\}, \tag{2c}$$

$$R_{i,h}^{0/+}(t) = \sigma_{i,h}^{0/+}\langle \nu_{th,h}\rangle \Big\{ \delta p_i(t)$$
$$\times \big[\delta p_i(t) - \delta n_i(t) - 2\delta N_i^-(t)\big]\Big\}. \tag{2d}$$

Then, we rewrote Eq. (11) in Ref. 34 in the time-dependent form shown in Eq. (3). The formulation of the negative-U center related carrier dynamics was built by combining Eqs. (2), (A2), and (A3)

$$\frac{d\delta n_i(t)}{dt} = -\Big[R_{i,e}^{0/-}(t) + R_{i,e}^{+/0}(t)\Big], \tag{3a}$$

$$\frac{d\delta p_i(t)}{dt} = -\Big[R_{i,h}^{-/0}(t) + R_{i,h}^{0/+}(t)\Big], \tag{3b}$$

$$\frac{d\delta N_i^-(t)}{dt} = R_{i,e}^{0/-}(t) - R_{i,h}^{-/0}(t). \tag{3c}$$

In actual experimental conditions, both E_1/E_2 related and DAP related pathways would occupy a certain proportion of the injection level g. Here, the portion of g corresponding to the E_1/E_2 channels is equal to the non-equilibrium carrier density at $t = 0$ (δn_0, δp_0) in the negative-U center related carrier dynamics modelling. The time-resolved PL intensity $I(t)$ of n-type 6H SiC at a low injection level, where $\delta n_0, \delta p_0 \ll n_0$, is considered to be proportional to the density of non-equilibrium minority carrier $\delta p(t)$, namely, $I(t) \propto \delta p(t)$. Hence, the PL lifetime is equivalent to the lifetime of non-equilibrium h^+ where $\tau_{PL}(t) \cong \tau_p(t)$. Note that the time-dependent h^+ lifetime is given by Eq. (4) where the expressions of hexagonal- and cubic-site-related h^+ lifetimes were included

$$\tau_p(t) = \left[-\frac{d\delta p(t)}{dt}\frac{1}{\delta p(t)}\right]^{-1}, \tag{4a}$$

$$\tau_{p,1}(t) = \left[-\frac{d\delta p_1(t)}{dt}\frac{1}{\delta p_1(t)}\right]^{-1}, \tag{4b}$$

$$\tau_{p,2}(t) = \left\{-\left[\frac{d\delta p_{2L}(t)}{dt} + \frac{d\delta p_{2H}(t)}{dt}\right]\frac{1}{\delta p_{2L}(t) + \delta p_{2H}(t)}\right\}^{-1}. \tag{4c}$$

The model was initialized by implementing $N_{u,i}$ and $\delta n_0(\delta p_0)$, where the related values were derived from the multi-phase exponential decay fitting of the experimental TRPL curve (will be introduced in Sec. IV B). The

simulations were executed using Simulink (MathWorks, Inc.) where the Bogacki-Shampine method[47] was implemented with a fixed time step of 10 ps.

B. Calculation of τ_{dap} by a steady-state recombination model

In the steady-state DAP recombination model demonstrated in Ref. 38, the DAP is treated as a single defect. The charge state S of this single defect, where the labelling is similar to that of Ref. 48, is designated by the number of occupied e^- as shown in Fig. 2. For example, the charge state $1'$ represents the excited state ready for e^--h^+ recombination via the DAP center, in which one e^- occupies the donor level while one h^+ occupies the acceptor level. The transfer of the minority carriers is crucial for DAP recombination. In Fig. 2, the solid arrows suggest the transfers of the minority carriers (e^-) in p-type 6H SiC where the minority carriers recombine with the majority carriers (h^+) on the perturbed acceptor level ($E_{a,p}$). The related charge state undergoes $S: 0 \to 1' \to 1$ and returns to state 0 after the recombination process. The dashed arrows suggest the transfers of the minority carriers (h^+) in n-type 6H SiC where minority carriers recombine with the majority carriers (e^-) on the perturbed donor level ($E_{d,p}^j$). Note that the subscripts "j" denote different lattice sites occupied by the nitrogen-induced donors [i.e., cubic 1 (c_1), cubic 2 (c_2), and hexagonal (h) sites]. The related charge state undergoes $S: 2 \to 1' \to 1$ followed by a return to state 2 after the recombination process.
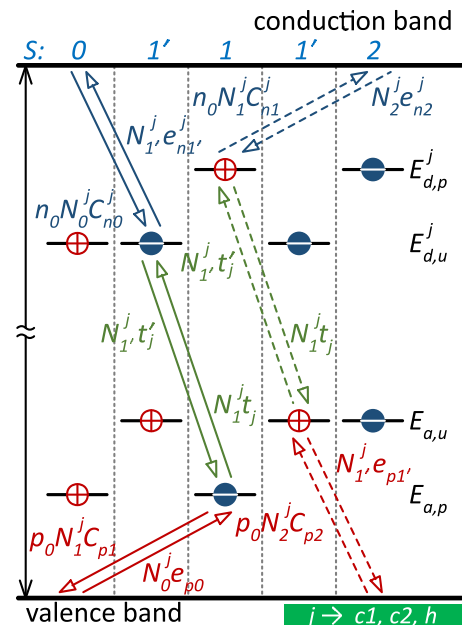

FIG. 2. A schematic band diagram of carrier generation or recombination via DAP, where S represents the charge state of the pair and there are five charge states in total separated by the gray dashed lines. The perturbed donor level or acceptor level is indicated by $E_{d,p}^j$ or $E_{a,p}$, whereas the unperturbed donor level or acceptor level is indicated by $E_{d,u}^j$ or $E_{a,u}$, respectively, where the subscripts "j" indicate different lattice sites occupied by the nitrogen-induced donors, namely, cubic 1 (c_1), cubic 2 (c_2), and hexagonal (h) sites. The path consisting of solid arrows designates the recombination scheme of the strongly p-type 6H SiC, while the path consisting of dashed arrows designates the recombination scheme of the strongly n-type 6H SiC.

The energy depths of the unperturbed donor level ($E_{d,u}^j$) and the unperturbed acceptor level (D-center, $E_{a,u}$) are indicated by ΔE_j ($j = c1, c2, h$) and ΔE_D shown in Table. II, where $c1(c2)$ and h represent the cubic- and hexagonal-site related donor levels, respectively. The energy difference between each pair of the perturbed/unperturbed level is actually the Coulomb interaction energy $U_E = e^2/(4\pi\varepsilon_0\varepsilon_r r_{dap})$, where e, ε_0, and ε_r designate the elementary charge, the vacuum permittivity, and the relative permittivity of 6H SiC, respectively. In particular, the transfers of the minority carriers involve the carrier capture/emission of the DAP at a certain charge state, e.g., $n_0 N_1^j C_{n1}^j$ indicates the e^- capture rate of the state 1, where N_1^j/C_{n1}^j is the density/e^- capture probability of the state 1 of the donor level E_j. Likewise, $N_2^j e_{n2}^j$ indicates the e^- emission rate of state 2 where e_{n2}^j represents the related h^+ emission probability. The transition probability of $1' \rightarrow 1$ or $1 \rightarrow 1'$ related to each donor level is symbolized by t_j' or t_j, respectively. Since it is the $1' \rightarrow 1$ transition that induces DAP recombination, the net steady-state recombination rate R_{dap} is

given by $R_{dap} = \sum_j N_{1'}^j t_j' - N_1^j t_j$. Here, R_{dap} can be rewritten in the more general form[38] as shown in Eq. (5), where $R_{0\rightarrow1'}^j$ and $R_{2\rightarrow1'}^j$ represent the net transition rate of $0 \rightarrow 1'$ and $2 \rightarrow 1'$, respectively. The derivation of the general conditions of the steady-state DAP recombination modelling based on Eq. (5) is described in Appendix B

$$R_{dap} = \sum_j R_{0\rightarrow1'}^j + R_{2\rightarrow1'}^j. \tag{5}$$

For the extrinsic n-type case in this research, the DAP lifetime is actually equivalent to the minority carrier lifetime, that is, $\tau_{dap} \approx \tau_p$. We further applied the condition of a small injection level and simplified the calculation by reconsidering the steady-state equilibrium of DAP recombination, where we let $C_{n0}^j = C_{p2} = C_p$ and $C_{n1}^j = C_{p1} = C_n^j$ for our condition of strong n-type 6H SiC. Then, we rewrote Eq. (22) in Ref. 38 for the extrinsic n-type case for each donor-site-dependent DAP as shown in the following equation:

$$\tau_{dap}^j = \frac{1}{n_0 N_{eff}^j W_j(r_{dap})}$$
$$\times \frac{\left[n_0 p_{a,u}\left(n_0 + n_{d,p}^j\right)\right]C_{n,j}^2 + \left[p_{a,u}\left(p_{a,p} + n_{d,p}^j\right)\left(n_0 + n_{d,p}^j\right)\right]C_p C_{n,j} + n_0 W_j(r_{dap})\left[\left(n_0 + n_{d,p}^j\right)C_{n,j} + p_{a,p}C_p\right]}{n_0 C_{n,j}^2 + C_p C_{n,j}\left(n_{d,p}^j + p_{a,p}\right)}. \tag{6}$$

The ratio between the donor level concentrations on hexagonal and cubic sites is considered[49] to be identical to the ratio of the number of hexagonal and cubic sites in the crystal lattices, where $N_h/N_c = 1 : 2$ (subscripts "h": hexagonal and "c": cubic) for 6H SiC. We further assumed that the number of $c1$ and $c2$ sites is equal, implying the same donor level concentration related to h, $c1$, and $c2$ sites. Accordingly, the mean DAP recombination lifetime of the separate recombination processes is calculated by the following equation:

$$\tau_{dap} = \frac{\sum_j (\tau_{dap}^j)^2}{\sum_j \tau_{dap}^j}. \tag{7}$$

IV. RESULTS AND DISCUSSION

The measured TRPL results of the three samples were summarized in Fig. 3. The scattered data points indicate the mean time-resolved PL intensities. For sample BK, four-phase exponential decay fitting [$y_0 + \sum_n^4 A_n \exp(-t/t_n)$] was applied on the experimental TRPL. Accordingly, the experimental TRPL data of two f-SiC samples were fitted with a three-phase exponential decay function [$y_0 + \sum_n^3 A_n \exp(-t/t_n)$].

A. The fastest and slowest TRPL decay channels in sample BK

The fitting on the TRPL of sample BK suggests that there are four decay channels for non-equilibrium carriers where we obtained $t_1 = 3$ ns and $A_1 = 56.1\%$ for the fastest

channel. One probable explanation for the carrier dynamics in this channel could be the combined effect from both Auger recombination (AR) and bimolecular recombination (BR) in the 6H SiC substrate.[50] At low injection levels ($g \ll n_0$), the lifetime of either AR or BR is limited by the doping level. The lifetime of AR is $\tau_{AR} = 1/(\gamma_e n_0^2)$, where γ_e is the Auger recombination coefficient for $e^- - e^- - h^+$ recombination in n-type semiconductors and typically $\gamma_e \approx (3.0\pm0.5) \times 10^{-29}$ cm^6 s^{-1} for 6H SiC.[51] The lifetime of BR is given by $\tau_{BR} = 1/(\gamma_B n_0)$, where γ_B is the bimolecular recombination coefficient which has a typical value in the range of $\times 10^{-11} \sim \times 10^{-12}$ cm^{-3} s^{-1} for 4H SiC.[51,52] The lifetime of the rapid decay at the initial stage (τ_{rapid}) for the n-type 6H SiC substrate follows the relation $1/\tau_{rapid} = 1/\tau_{AR} + 1/\tau_{BR}$.[50] By assuming that γ_B of 6H SiC is comparable to that of 4H SiC, the estimated τ_{rapid} could be comparable to t_1, i.e., within the same order of magnitude. Hence, the origin of the fastest channel still requires further investigation.

The nature of the fourth channel in sample BK ($t_4 = 4.801$ μs and $A_4 = 1.2\%$) is still unknown. We confirmed by steady state modeling that the DAP recommendation process is much slower than this time constant (see details in Appendix C). This does not mean that no DAP recombination occurs in sample BK; instead, the decay channel related to DAP recombination is believed to occupy the proportion of non-equilibrium carriers less than A_4 with a longer lifetime than t_4, where the background noise has obscured this decay channel during the TRPL measurements. Additionally, the effect of surface recombination cannot correspond to this channel either. Let us consider the fundamental
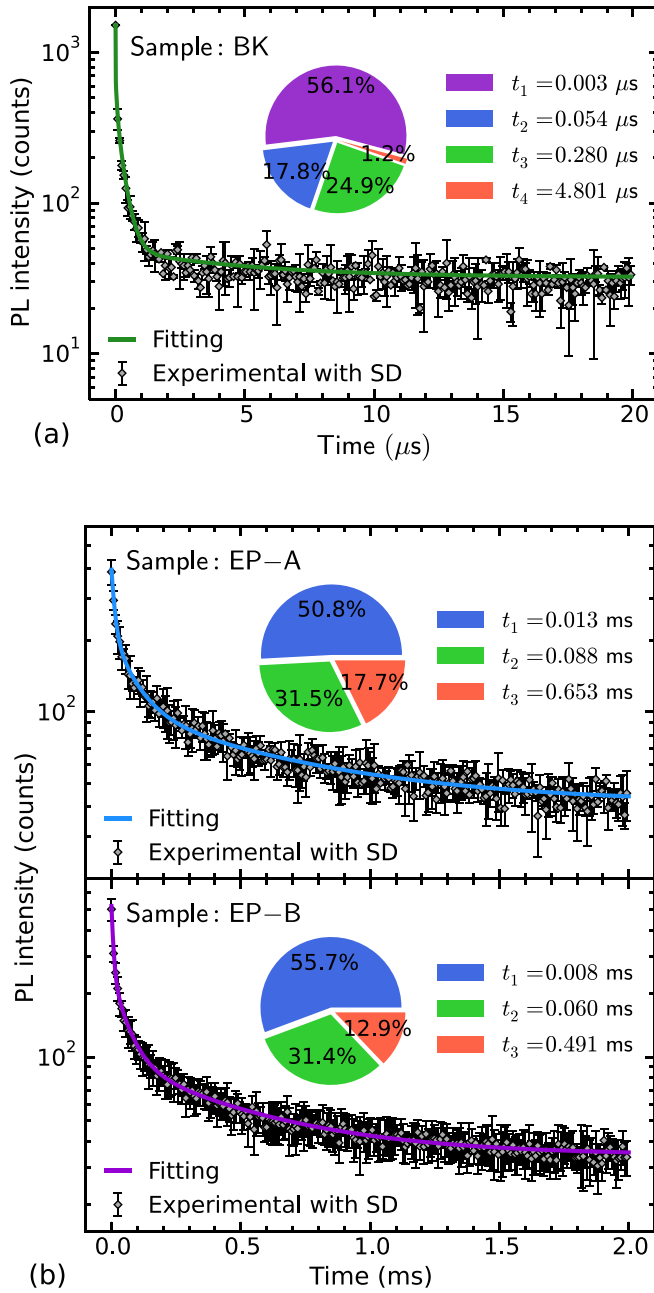
FIG. 3. TRPL decays recorded via TCSPC histograms (a) for sample BK and (b) for samples EP-A and EP-B. Each error bar indicates the standard deviation (SD) of the measured photon count at a certain time point, whereas the solid line represents the four-phase (for sample BK) or three-phase (for samples EP-A and EP-B) exponential decay fitting. The normalized amplitudes A_i are summarized in the pie chart, where the time constants t_i for each A_i are marked in the legends.

surface recombination lifetime (τ_s)[53] in sample BK where $\tau_s = d^2/(D\pi^2)$. The diffusion constant $D = 2.5$ cm^2 s^{-1} for hole diffusion in 6H SiC is available from Ref. 54, from which we obtain a lower bound on τ_s[53] for the sample BK of $\sim 42.8\,\mu$s which is still one order of magnitude higher than t_4.

B. Negative-*U* center related TRPL decay channels

The second and third decay channels in sample BK were considered to be associated with the negative-*U* center related carrier dynamics. As Ikeda *et al.* (Ref. 55) have

experimentally demonstrated, the density ratio between the nitrogen-induced donors on hexagonal and cubic sites $(N_h : N_c)$ could be roughly treated as 1:2. Based on this correspondence, we believed that the amount of hexagonal-site-related E_1 centers should be smaller than the amount of cubic-site-related E_{2L} and E_{2H} centers. Yet it may not strictly obey the 1:2 relation. Accordingly, one of those two negative-*U* center related decay channels with larger amplitude A_i, which means taking over more non-equilibrium carriers, ought to be related to the cubic defect centers (E_{2L} and E_{2H}). Hence, the injection level allocated to the second channel was set to A_2g where the density of the E_1 center was calculated using Eq. (1). Since the third channel is shared by two defect centers on cubic sites and we have assumed that these two centers have identical densities, we obtain simultaneously the defect density for both centers as $N_{u,2L}, N_{u,2H} = 2/[(\sigma_{2L,h} + \sigma_{2H,h})\langle\nu_{th,h}\rangle t_2]$, assuming that either of the defect centers took over half of the injection level ($A_3g/2$).

The exponential decay fitting of the TRPL of both f-SiC samples (EP-A and EP-B) shows that there are three decay channels for f-SiC. By modelling the first and second channels based on the negative-*U* center related carrier dynamics, it was found that the simulated PL decay curve agreed well with the corresponding fast decay part of each measured TRPL. Note that the allocated injection level for each channel and the densities of those three defect centers in the two samples were estimated using the same method mentioned above for sample BK. The third decay channels in both samples were believed to be related to the DAP recombination where the allocated injection level for the DAP recombination process was A_3g. Note that none of the decay channels in either f-SiC samples were attributed to surface recombination effects. The reason could be explained by the fact that the non-equilibrium carriers are hindered by the acceptor-induced space charge field at a low injection level $(g \ll N_a)$,[56–58] causing the diffusion coefficient D to be negligible. This will result in the fundamental surface recombination lifetime[53] being much longer than any extracted time constant from the TRPL measurements of both f-SiC samples.

The results of the carrier dynamics simulations are summarized in Figs. 4 and 5. In Fig. 4, for both f-SiC samples, the normalized density of the non-equilibrium minority (h^+) carriers, which was designated by $\delta p(t)/g = \sum_i \delta p_i(t)/g$ from the simulation, agreed quite well with the negative-*U* center related two-phase exponential decay extracted from the TRPL fitting. The simulated $\delta p(t)$ for sample BK showed a bit slower decay compared to the corresponding fitting curve, where this slight mismatch might be caused by the unknown defect centers, e.g., midgap defects in 6H SiC.[59] We can see that the negative-*U* center related carrier recombinations dominate the TRPL decay process before the time point indicated by the vertical dashed line [BK: 0.92 μs, EP-A(B): 60 μs] where the decay channel with the longest time constant starts to dominate. Furthermore, the defect-related TRPL decay can be divided into two stages, where the first stage reflects the joint effect from both cubic and hexagonal centers while only the slower decay channel is highlighted at the second stage. The lifetimes of the non-equilibrium h^+ for
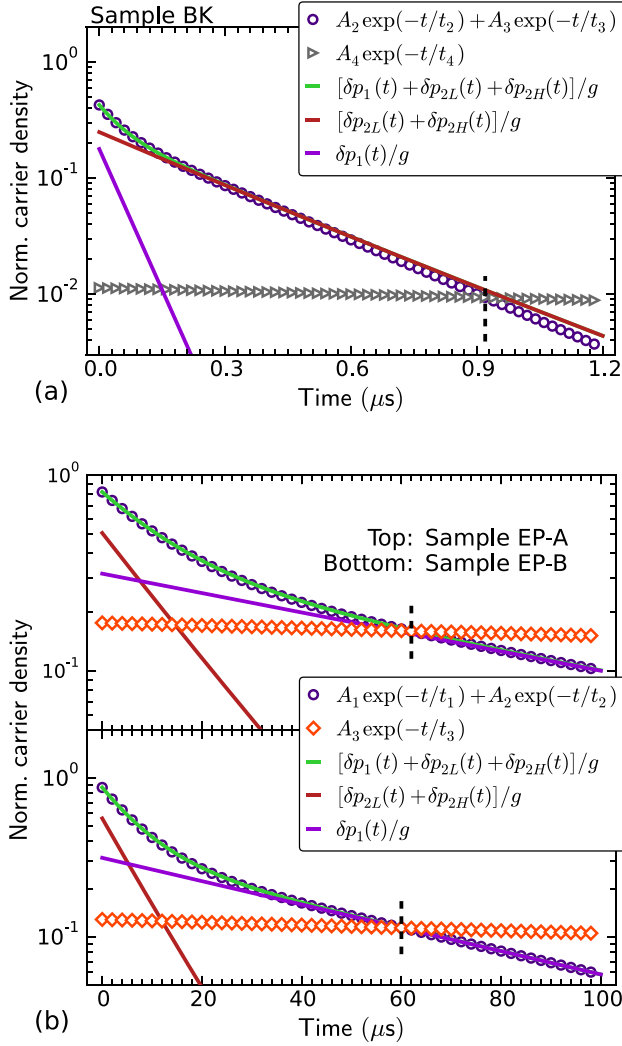
FIG. 4. Results of the negative U-center related carrier dynamics simulation for (a) sample BK and (b) samples EP-A and EP-B. The open circles designate the defect-related exponential decay components. The open triangles represent the decay channels with the longest time constant in the bulk 6H SiC sample. The open squares represent the decay channels related to DAP recombinations in two f-SiC samples. All the related A_n and t_n were extracted from Fig. 3. The three curves represent the time-dependent non-equilibrium h^+ densities corresponding to the overall negative U-centers, hexagonal site, and cubic site, where the time-resolved PL intensity $I(t) \propto \delta p(t)$.

different transition processes were also extracted from the carrier dynamics simulations and are summarized in Fig. 5. The overall, hexagonal- and cubic-site-related non-equilibrium h^+ lifetimes were calculated by Eq. (4), where the simulated $\tau_{p,1}(t)$ and $\tau_{p,2}(t)$ were found to be nearly time-independent and quite close to the corresponding time constants extracted from the TRPL fittings. Additionally, the above-mentioned two-stage distinction within the defect-related TRPL decay can be further confirmed considering the evolution of every $\tau_p(t)$ shown in Fig. 5. It can be seen that the evolution of $\tau_p(t)$ was influenced by both E_1 and E_2 related carrier dynamics at the early stage, while later it reached a longer lifetime between $\tau_{p,1}(t)$ and $\tau_{p,2}(t)$ and almost became time-independent.

C. Influence of negative-U centers on PL properties

In order to distinguish the contributions from the hole-involved charge state transitions $E_i^- \rightarrow E_i^0$ and $E_i^0 \rightarrow E_i^+$, we
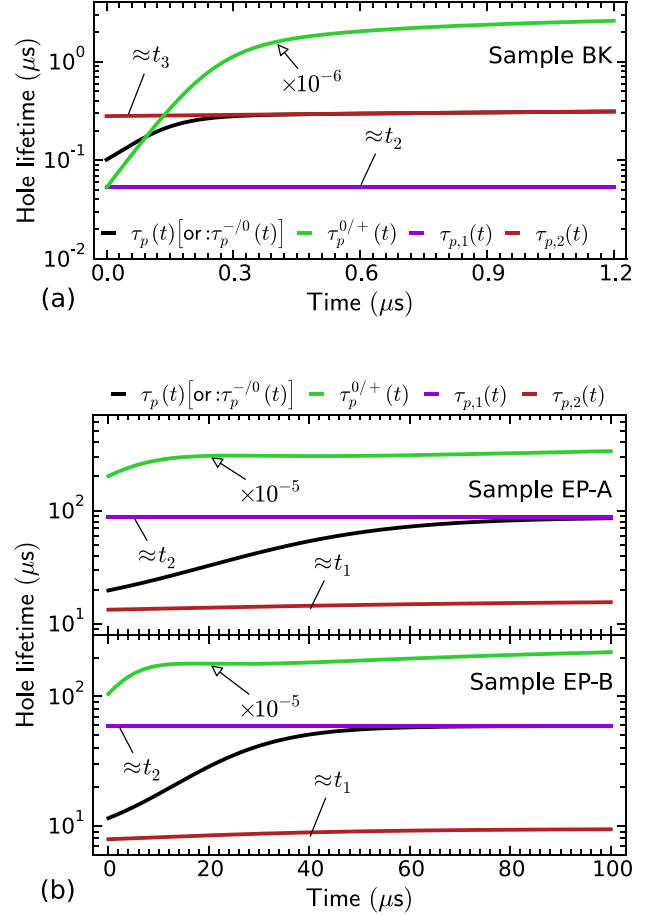

FIG. 5. Results of the negative U-center related carrier dynamics simulation for (a) sample BK and (b) samples EP-A and EP-B. Non-equilibrium h^+ lifetimes of the entirety ($\tau_p(t)$), the cubic- or hexagonal-site-related channel ($\tau_{p,1}(t)$ or $\tau_{p,2}(t)$), and the $E_i^- \rightarrow E_i^0$ or $E_i^0 \rightarrow E_i^+$ transition ($\tau_p^{-/0}(t)$, $\tau_p^{0/+}(t)$, respectively) related channel are presented.

introduced the "relative" h^+ lifetimes for either transition where $\tau_p^Q = [\sum_i |R_{i,h}^Q|/\delta p(t)]^{-1}$ with Q referring to "–/0" or "0/+." The simulated $\tau_p^{-/0}(t)$ and $\tau_p^{0/+}(t)$ for each sample are also included in Fig. 5. It was found that $\tau_p^{0/+}(t)$ for each sample was extremely long and has to be divided by 10^6 (for bulk SiC) or 10^5 (for f-SiC) in order to be presented with other carrier lifetimes in Fig. 5. Instead, $\tau_p^{-/0}(t)$ was found to be nearly identical to $\tau_p(t)$ for each sample, which means that the $E_i^- \rightarrow E_i^0$ transitions dominate the hole capture process. Since all three samples in this work are heavily doped n-type, the Fermi level of each sample is close to the conduction band minimum. In this case, for a negative-U system, the neutral carbon vacancy (E_i^0) is favored at thermodynamic equilibrium.[25] Hence, most of the E_i^0 states of the negative-U centers were not likely to transfer further to the E_i^+ states, causing the transition rate of $E_i^0 \rightarrow E_i^+$ to be extremely low.

It has been widely accepted that the E_1/E_2 centers are the carrier lifetime killers[60] and contribute to the non-radiative recombinations. This agreed with our observation that the absolute PL intensity shown in Fig. 6 for each sample was inversely correlated with the estimated density of the E_1/E_2 center (N_u) extracted from the respective TRPL measurement. The PL intensity of either EP-A or EP-B was ∼60 or ∼40 times higher than that of the bulk sample, respectively, and the
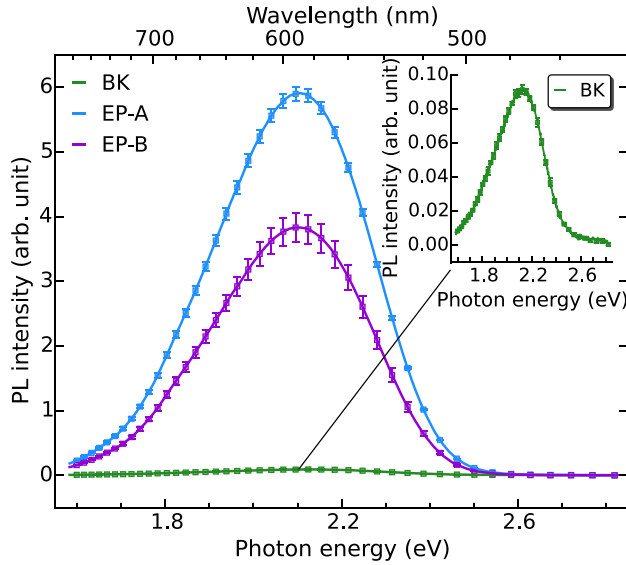
FIG. 6. Time-integrated PL intensity spectra of all three samples. Each error bar indicates the standard deviation (SD) at a certain wavelength, whereas each solid curve indicates the mean PL intensity. The inset is the zoom-in of the PL spectrum of sample BK.

N_u of either f-SiC sample was two orders of magnitude lower than latter's as shown in Table I. Here, we implemented a simple equation slightly modified from the original form[1] to evaluate the IQE (labelled as η_{int}) of our samples, where originally $\eta_{int} = 1/(1 + \tau_A/\tau_{nr})$ and $\tau_A | \tau_{nr}$ designate the h^+ relaxation time | the overall non-radiative lifetime separately. As we know $\tau_{dap} \approx \tau_p$ which was already mentioned in Sec. III B, τ_p actually represents the hole relaxation time equivalent to τ_A. Hence, in our case, $\eta_{int} = 1/(1 + \tau_{dap}/\tau_{nr})$. For two f-SiC samples, by applying $\tau_{dap} = t_3$ and $1/\tau_{nr} = 1/t_1 + 1/t_2$, the estimated IQE for samples EP-A and EP-B was found to be around 1.7% and 1.4%, respectively. For sample BK, since the fourth decay channel with the longest time constant cannot be attributed to DAP recombination (see Sec. IV A for the related discussion), estimation of its IQE is unavailable; nonetheless, a rather low value of IQE compared to f-SiC samples can be expected. To summarize how the E_1/E_2 defects could affect the IQE of our samples, we can see from Fig. 3 that higher E_1/E_2 densities enlarge the difference between the E_1/E_2 related and DAP related injection levels and cause τ_{nr} to be shorter. On the contrary, less non-equilibrium carriers are occupied by DAP related pathways, leading to lower intensity of DAP related luminescence. The trends on the pathways of both E_1/E_2 and DAP would eventually result in lower IQE.

D. Comparison between EP-A and EP-B

Typically, the DAP recombination decay is described in the form of t^{-m} rather than a single exponential decay process, where t and m designate the time and the power factor of decay, respectively.[61] The above-mentioned methodology is suitable for modelling the DAP-related PL decay under high excitation power, where the effective DAP separation distance could change dramatically during the transient measurement period. However, our TRPL measurements were launched at a low injection level ($g \ll n_0$) where the initial

DAP separation distance was already quite long compared with the average Bohr radius ($\sum_j a_0^j/3$) of the donors; therefore, the steady-state DAP recombination model was applied here to explain the DAP recombination process. The simulation results of the steady-state DAP recombination of the two f-SiC samples are summarized in Fig. 7 where the injection level allocated for either sample was set to A_3g extracted from the fitting results in Fig. 3. The average DAP separation distances were calculated to be 3.79 times (EP-A) and 3.54 times (EP-B) the average Bohr radius of donors. It was believed that the shorter r_{dap} of EP-B, which means denser DAP, was caused by its higher dopant concentration. The contrast between these two average r_{dap} agreed well with the recognized trend of DAP lifetime, where the longer DAP separation distance could result in the lower DAP transition probability [see Eq. (B5)] and meanwhile cause longer DAP recombination lifetime.[61,62]

It was found that a higher portion of injection level was allocated to EP-A (17.7%) than that of EP-B (12.9%) as shown in Fig. 3, which caused the former's integrated PL intensity approximately 50% higher than the latter's (see Fig. 6). On the contrary, from Fig. 3, we can see that a 4.8% more portion of non-equilibrium carriers, which was almost 40% of the amount for EP-B's DAP channel, were enrolled in the negative-U center related carrier pathways in EP-B. Apparently, this was caused by the higher density of E_1/E_2 in EP-B than in EP-A as shown in Table I. As a result, we can see that EP-B had higher DAP transition probability (i.e., shorter average r_{dap}) but lower IQE than EP-A as mentioned in Sec. IV C. We believed that the higher E_1/E_2 defect density in sample EP-B came along with the higher nitrogen dopant compared with sample EP-A[63] if the C/Si ratio was
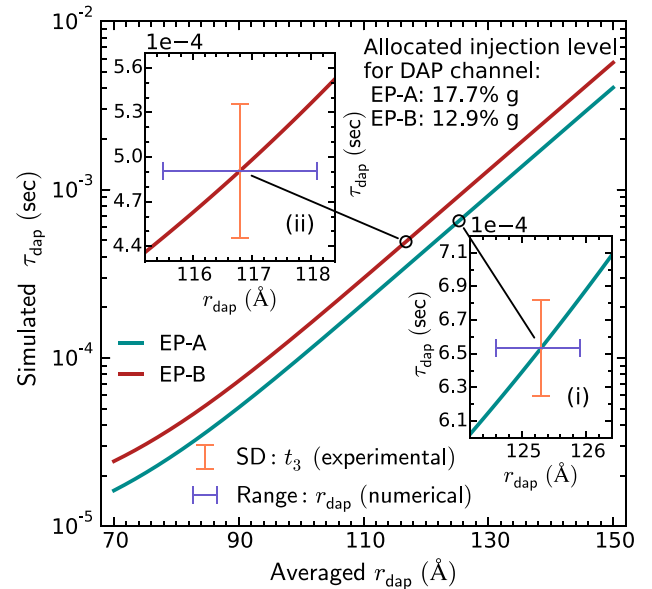

FIG. 7. Results of the pair-separation-dependent (r_{dap}) DAP lifetime simulation of samples EP-A and EP-B. In the main graph, the values on the y-axis of the circled points are derived from t_3 of each f-SiC sample in Fig. 3, whereas the corresponding values on the x-axis indicate the calculated r_{dap}. In each inset, the error bar along the y-axis indicates the standard deviation of the fitted DAP lifetime, whereas the error bar along the x-axis indicates the corresponding range of the calculated DAP separation (r_{dap}).

controlled within a proper range. Otherwise, too low C/Si ratio could facilitate the formation of 3C SiC[64] while too high C/Si ratio could induce the high graphitization of the source.[33] In addition, it was found that C/Si ratio itself could also affect the density of negative-U centers, e.g., the density of the Z_1/Z_2 centers in the 4H SiC epilayer was found to decrease monotonically in the range of C/Si ratio of 0.5–2.0.[65] On the other hand, the formation of the E_1/E_2 related carbon vacancies could degrade the doping efficiency,[66,67] where the large proportion of the donor impurities in SiC samples might be compensated.[68,69] To summarize, reducing the formation of the E_1/E_2 defects in f-SiC needs to be taken into consideration to find the new trade-off when optimizing the C/Si ratio during the epilayer growth. Furthermore, despite the fact that the concentration of the nitrogen dopant in f-SiC should be kept high enough ($>10^{18}$ cm^{-3}) to ensure the large density of DAP recombination,[1] the nitrogen doping still requires further study to narrow down its range.

V. CONCLUSIONS

We have characterized two f-SiC samples with identical epilayer thicknesses and one bulk 6H SiC substrate by applying TRPL and static PL measurements in which all the samples are heavily nitrogen-boron co-doped and n-type. An apparent trend was found that slower TRPL decay was accompanied by higher measured PL intensity. Negative-U center (E_1/E_2 defect) related carrier dynamics modelling and steady-state DAP recombination simulation were applied to the TRPL. The results of the carrier dynamics modelling revealed that the density of the E_1/E_2 defects in bulk 6H SiC was found to be two orders of magnitude higher than that of either f-SiC epilayer. In addition, the ultrafast decay channel with the time constant of ~3 ns was extracted from the TRPL curve of the bulk substrate. This fast decay might be due to the joint effect from both Auger recombination and bimolecular recombination where both of the processes are considered as non-radiative. It is believed that the extra non-radiative decay channel and the much higher E_1/E_2 concentration in the bulk substrate caused quite lower PL intensity and IQE than those in the two f-SiC samples. The results of the steady-state DAP simulations on the f-SiC samples indicate that both the calculated average DAP separation distances (r_{dap}) were three times larger than the average Bohr radius of an electron (captured by a neutral donor) at the low injection level (order: $\times 10^{11}$ cm^{-3}). The longer r_{dap} was found to result in a longer DAP recombination lifetime. Sample EP-B with a slightly higher density of E_1/E_2 defects was found to show more rapid TRPL decay and weaker static PL intensity along with lower IQE than sample EP-A. We believe that the C/Si ratio and the nitrogen doping level during the f-SiC epilayer growth still require further optimization to find the new trade-off between less E_1/E_2 defects and other indicators of the crystal quality, e.g., the extent of the graphitization of the source.

APPENDIX A: NEGATIVE-U CENTER RELATED CARRIER DYNAMICS—GENERAL CONDITIONS

As shown in Fig. 1, each dashed arrow originates from the provider (conduction band/D-center) of the non-equilibrium carriers towards the corresponding charge state transition, where the related carrier capture rate was expressed in Eq. (A1) which was rewritten from Eq. (9) in Ref. 34

$$R_{i,e}^{0/-}(t) = \sigma_{i,e}^{0/-} \langle \nu_{th,e} \rangle \left\{ [n_0 + \delta n_i(t)]N_i^0(t) - n_i^{0/-}N_i^-(t) \right\},$$
(A1a)

$$R_{i,e}^{+/0}(t) = \sigma_{i,e}^{+/0} \langle \nu_{th,e} \rangle \left\{ [n_0 + \delta n_i(t)]N_i^+(t) - n_i^{+/0}N_i^0(t) \right\},$$
(A1b)

$$R_{i,h}^{-/0}(t) = \sigma_{i,h}^{-/0} \langle \nu_{th,h} \rangle \left\{ [p_0 + \delta p_i(t)]N_i^-(t) - p_i^{-/0}N_i^0(t) \right\},$$
(A1c)

$$R_{i,h}^{0/+}(t) = \sigma_{i,h}^{0/+} \langle \nu_{th,h} \rangle \left\{ [p_0 + \delta p_i(t)]N_i^0(t) - p_i^{0/+}N_i^+(t) \right\}.$$
(A1d)

The equilibrium e^-, h^+ concentration was symbolized by n_0, p_0. The mean thermal velocity of e^- or h^- was represented by $\langle \nu_{th,e(h)} \rangle = (3k_b T/m_{e(h)}^*)^{0.5}$. The non-equilibrium e^-, h^+ density as a function of time (t) was designated as $\delta n_i(t), \delta p_i(t)$, where the subscript "$i$" ($i \Rightarrow 1, 2L, 2H$) denotes the component of the negative-U system: E_1, E_{2L}, or E_{2H}. The total non-equilibrium carrier density (e^- or h^+) at the certain time t can be expressed by $\delta n(t), \delta p(t) = \sum_i \delta n_i(t), \sum_i \delta p_i(t)$. The expressions of $n_i^{0/-}, n_i^{+/0}$ are given by[70] $n_i^{0/-}, n_i^{+/0} = N_c \exp[-\Delta E_i^L/(k_b T)]$ (L: $0/-$ or $+/0$), where N_c is the effective density of states in the conduction band (cm^{-3}), while the expressions of $p_i^{-/0}, p_i^{0/+}$ can be roughly estimated by $N_a \exp[-(E_g - \Delta E_i^L - \Delta E_D)/(k_b T)]$ (L: $-/0$ or $0/+$).

The time-varying density of negative-U center i with a charge state of C is designated as $N_i^C(t)$ (C: $-$, 0, $+$), where the total density of the negative-U center[34] at time t is $N_u = \sum_i \sum_C N_i^C(t)$. Similarly, the net change of the charge state E_i^C variation of one negative U center should be equal to zero[34] at any time t

$$\sum_C \delta N_i^C(t) = 0,$$
(A2)

where $\delta N_i^C(t) = N_i^C(t) - N_{i0}^C$ represents the time-dependent density change of the charge state "C," and N_{i0}^C designates

the initial density of the charge state "C." Note that at RT, all three centers are in the E_i^- state, which means $N_{i0}^+, N_{i0}^0 = 0$ and $N_{i0}^- = N_{u,i}$. By reconsidering the charge state transfer via e^- capture[20] $E_i^- \rightarrow E_i^0 + e^- \rightarrow E_i^+ + 2e^-$, the net density of non-equilibrium e^- (majority carriers) is given by

$$\delta n_i(t) - \delta p_i(t) = \delta N_i^0(t) + 2\delta N_i^+(t). \quad \text{(A3)}$$

APPENDIX B: STEADY-STATE DAP RECOMBINATION CALCULATION—GENERAL CONDITIONS

As shown in Fig. 2, the dashed | solid pathways indicate the dominating DAP recombination channel for n-type | p-type 6H SiC, where the carrier capture/emission would reach equilibrium in the steady-state. Therefore, based on Eq. (5), we can summarize the condition for the steady-state DAP recombination as shown in Eq. (B1). Note that N_{eff}^j designates the effective e^--h^+ pair concentration related to each donor site for DAP recombination in which N_{eff}^j is dependent on the density of e^- at each donor state E_j.[9] Here, we derived N_{eff}^j from the allocated injection level for DAP recombination g_{dap} and the static Fermi level E_F using Eq. (B2). It is worthwhile mentioning that at such a low injection level ($\sim \times 10^{11}$ cm^{-3}), the quasi-Fermi level for e^- is almost identical to the static Fermi level E_F. The calculation of E_F was derived from Ref. 36

$$p_0 N_1^j C_{p1} - N_0^j e_{p0} = R_{0\rightarrow 1'}^j, \quad \text{(B1a)}$$

$$p_0 N_2^j C_{p2} - N_{1'}^j e_{p1'} = R_{2\rightarrow 1'}^j, \quad \text{(B1b)}$$

$$t_j' N_{1'}^j - t_j N_1^j = R_{0\rightarrow 1'}^j + R_{2\rightarrow 1'}^j, \quad \text{(B1c)}$$

$$N_{1'}^j e_{n1'}^j + p_0 N_1^j C_{p1} - \left(e_{p0} + n_0 C_{n0}^j\right) N_0^j = 0, \quad \text{(B1d)}$$

$$N_{1'}^j e_{p1'} + n_0 N_1^j C_{n1}^j - \left(e_{n2}^j + p_0 C_{p2}\right) N_2^j = 0, \quad \text{(B1e)}$$

$$\sum_S N_S^j = N_{\text{eff}}^j, \quad \text{(B1f)}$$

$$N_{\text{eff}}^j = \frac{g_{\text{dap}}}{1 + 1/g_D \exp\left((E_g - \Delta E_j - E_F)/(k_b T)\right)}. \quad \text{(B2)}$$

Here, we introduced four auxiliary parameters shown in Eq. (B3) that represent the carrier densities at each perturbed/unperturbed donor/acceptor level by treating these levels as pseudo-Fermi levels temporarily. The emission probabilities in Eq. (B1) could be derived from the capture probabilities related to the reversed paths by applying the parameters obtained from Eq. (B3), where $e_{n1'}^j = n_{d,u} C_{n0}^j$, $e_{n2}^j = n_{d,p} C_{n1}^j$, $e_{p0} = p_{a,p} C_{p1}$, and $e_{p1'} = p_{a,u} C_{p2}$

$$n_{d,p}^j = n_0 \exp\left(\frac{E_g - \Delta E_j - E_F}{k_b T}\right), \quad \text{(B3a)}$$

$$n_{d,u}^j = n_0 \exp\left(\frac{E_g - \Delta E_j + U_E(r_{\text{dap}}) - E_F}{k_b T}\right), \quad \text{(B3b)}$$

$$p_{a,p} = p_0 \exp\left(\frac{E_F - \Delta E_D}{k_b T}\right), \quad \text{(B3c)}$$

$$p_{a,u} = p_0 \exp\left(\frac{E_F - \Delta E_D - U_E(r_{\text{dap}})}{k_b T}\right). \quad \text{(B3d)}$$

Since the relation between t_j and t_j' follows Eq. (B4), it can be deduced that $t_j' \gg t_j$ at RT. Now, t_j' can be treated as the net DAP transition probability where it is preferable to relabel t_j' into the more general form, namely, $W(r_{\text{dap}})$. Here, we adopted the expression of $W(r_{\text{dap}})$ from Ref. 71 shown in Eq. (B5), which is suitable for the DAP transitions with strong phonon replicas. Hagen et al. (Ref. 62) experimentally found that W_0 of 6H SiC should be $(3–4) \times 10^5$ s^{-1}. Here, we applied $W_0 = 3.5 \times 10^5$ s^{-1}. a_0^j denotes the Bohr radius related to different donor levels in 6H SiC using Eq. (B6)[43]

$$\frac{t_j'}{t_j} = \exp\left(\frac{\Delta E_j + \Delta E_D + U_E(r_{\text{dap}})}{k_b T}\right), \quad \text{(B4)}$$

$$W_j(r_{\text{dap}}) = W_0 \exp\left(-\frac{2r_{\text{dap}}}{a_0^j}\right), \quad \text{(B5)}$$

$$a_0^j = \left(\frac{eh^2}{8\pi^2 m_e^*(\varepsilon_0 \varepsilon_r)^2} \frac{1}{\Delta E_j^3}\right)^{1/4}. \quad \text{(B6)}$$

APPENDIX C: SIMULATION OF τ_{dap} OF SAMPLE BK WITH DIFFERENT INJECTION LEVELS g

The simulation results of τ_{dap} of sample BK are summarized in Fig. 8, where 1%, 5%, and 10% to 100% (with 10%
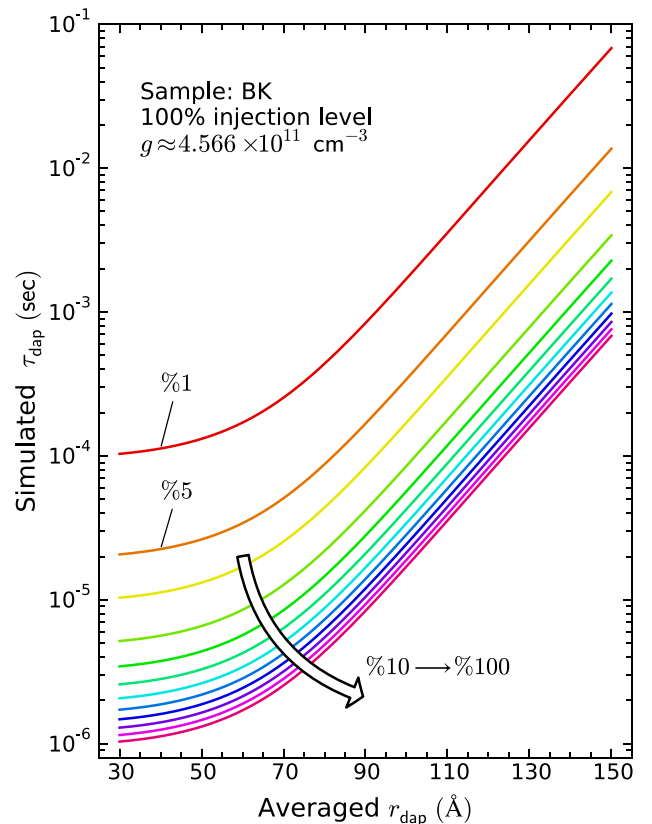

FIG. 8. Simulated τ_{dap} of sample BK. The proportion of the non-equilibrium carriers for DAP recombination varies from 1% to 100% of the injection level.

interval) of the injection level g were allocated to the channel of the DAP recombination in each simulation. The results suggest that τ_{dap} decreases with increasing injection level g. We can see that the calculated τ_{dap} was longer than $20\,\mu s$ assuming that 5% of g was allocated to the DAP recombination channel. Therefore, one can expect that the related τ_{dap} should be even longer than $20\,\mu s$ if the fourth recombination channel in sample BK (with $A_4 = 1.2\%$, see Fig. 3) was treated as the DAP recombination channel. Considering the fact that the fourth recombination channel in sample BK has a lifetime of $4.801\,\mu s$ (see Fig. 3), it is not related to the DAP recombination channel.

[1]S. Kamiyama, T. Maeda, Y. Nakamura, M. Iwaya, H. Amano, I. Akasaki, H. Kinoshita, T. Furusho, M. Yoshimoto, T. Kimoto, J. Suda, A. Henry, I. G. Ivanov, J. P. Bergman, B. Monemar, T. Onuma, and S. F. Chichibu, J. Appl. Phys. **99**, 093108 (2006).

[2]S. Kamiyama, M. Iwaya, T. Takeuchi, I. Akasaki, R. Yakimova, and M. Syväjärvi, Thin Solid Films **522**, 23 (2012).

[3]H. Ou, Y. Ou, A. Argyraki, S. Schimmel, M. Kaiser, P. Wellmann, M. K. Linnarsson, V. Jokubavicius, J. Sun, R. Liljedahl, and M. Syväjärvi, Eur. Phys. J. B **87**, 58 (2014).

[4]S. Kamiyama, M. Iwaya, T. Takeuchi, I. Akasaki, M. Syväjärvi, and R. Yakimova, J. Semicond. **32**, 013004 (2011).

[5]M. Syväjärvi, J. Müller, J. Sun, V. Grivickas, Y. Ou, V. Jokubavicius, P. Hens, M. Kaisr, K. Ariyawong, K. Gulbinas, P. Hens, R. Liljedahl, M. K. Linnarsson, S. Kamiyama, P. Wellmann, E. Spiecker, and H. Ou, Phys. Scr. **T148**, 014002 (2012).

[6]Y. Ou, V. Jokubavicius, R. Yakimova, M. Syväjärvi, and H. Ou, Opt. Lett. **37**, 3816 (2012).

[7]Y. Ou, X. Zhu, V. Jokubavicius, R. Yakimova, N. A. Mortensen, M. Syväjärvi, S. Xiao, and H. Ou, Sci. Rep. **4**, 4662 (2014).

[8]W. Lu, Y. Ou, E. M. Fiordaliso, Y. Iwasa, V. Jokubavicius, M. Syväjärvi, S. Kamiyama, P. M. Petersen, and H. Ou, Sci. Rep. **7**, 9798 (2017).

[9]Y. Ou, V. Jokubavicius, S. Kamiyama, C. Liu, R. W. Berg, M. Linnarsson, R. Yakimova, M. Syväjärvi, and H. Ou, Opt. Mater. Express **1**, 1439 (2011).

[10]J. W. Sun, V. Jokubavicius, R. Liljedahl, R. Yakimova, S. Juillaguet, J. Camassel, S. Kamiyama, and M. Syväjärvi, Thin Solid Films **522**, 33 (2012).

[11]G. Manolis, K. Gulbinas, V. Grivickas, V. Jokubavicius, M. K. Linnarsson, and M. Syväjärvi, IOP Conf. Ser.: Mater. Sci. Eng. **56**, 012006 (2014).

[12]S. Schimmel, M. Kaiser, V. Jokubavicius, Y. Ou, P. Hens, M. K. Linnarsson, J. Sun, R. Liljedahl, H. Ou, M. Syväjärvi, and P. Wellmann, IOP Conf. Ser.: Mater. Sci. Eng. **56**, 012002 (2014).

[13]M. Aboelfotoh and J. Doyle, Phys. Rev. B **59**, 10823 (1999).

[14]T. Dalibor, G. Pensl, H. Matsunami, T. Kimoto, W. J. Choyke, A. Schöner, and N. Nordell, Phys. Status Solidi A **162**, 199 (1997).

[15]S. Sasaki, K. Kawahara, G. Feng, G. Alfieri, and T. Kimoto, J. Appl. Phys. **109**, 013705 (2011).

[16]M. Weidner, T. Frank, G. Pensl, A. Kawasuso, H. Itoh, and R. Krause-Rehberg, Physica B **308–310**, 633 (2001).

[17]G. Pensl, T. Frank, M. Krieger, M. Laube, S. Reshanov, F. Schmid, and M. Weidner, Physica B **340–342**, 121 (2003).

[18]X. D. Chen, C. L. Yang, M. Gong, W. K. Ge, S. Fung, C. D. Beling, J. N. Wang, M. K. Lui, and C. C. Ling, Phys. Rev. Lett. **92**, 125504 (2004).

[19]C. Hemmingsson, N. T. Son, O. Kordina, E. Janzén, and J. L. Lindström, J. Appl. Phys. **84**, 704 (1998).

[20]C. G. Hemmingsson, N. T. Son, and E. Janzén, Appl. Phys. Lett. **74**, 839 (1999).

[21]G. D. Watkins and J. R. Troxell, Phys. Rev. Lett. **44**, 593 (1980).

[22]G. A. Baraff, E. O. Kane, and M. Schlüter, Phys. Rev. Lett. **43**, 956 (1979).

[23]P. W. Anderson, Phys. Rev. Lett. **34**, 953 (1975).

[24]F. Bechstedt, A. Zywietz, and J. Furthmüller, Europhys. Lett. **44**, 309 (1998).

[25]A. Zywietz, J. Furthmüller, and F. Bechstedt, Phys. Rev. B **59**, 15166 (1999).

[26]M. Gong, S. Fung, C. D. Beling, and Z. You, J. Appl. Phys. **85**, 7604 (1999).

[27]A. A. Lebedev, A. I. Veinger, and D. V. Davydov, J. Appl. Phys. **88**, 6265 (2000).

[28]A. Kurtz, E. Muñoz, J. M. Chauveau, and A. Hierro, J. Phys. D **50**, 065104 (2017).

[29]M. Lades, "Modeling and simulation of wide bandgap semiconductor devices: 4H/6H-SiC," Ph.D. thesis (Technische Universität München, 2000).

[30]J. P. Bergman, O. Kordina, and E. Janzén, Phys. Status Solidi A **162**, 65 (1997).

[31]J. P. Bergman, Diamond Relat. Mater. **6**, 1324 (1997).

[32]M. Syväjärvi and R. Yakimova, in *Comprehensive Semiconductor Science and Technology*, edited by P. Bhattacharya, R. Fornari, and H. Kamimura (Elsevier, Amsterdam, 2011), pp. 202–231.

[33]V. Jokubavicius, P. Hens, R. Liljedahl, J. W. Sun, M. Kaiser, P. Wellmann, S. Sano, R. Yakimova, S. Kamiyama, and M. Syväjärvi, Thin Solid Films **522**, 7 (2012).

[34]P. B. Klein, J. Appl. Phys. **103**, 033702 (2008).

[35]S. Sridhara, T. Eperjesi, R. Devaty, and W. Choyke, Mater. Sci. Eng. B **61–62**, 229 (1999).

[36]V. Zeghbroeck, *Principles of Semiconductor Devices and Heterojunctions* (Prentice Hall PTR, 2007).

[37]E. Janzén, A. Gali, A. Henry, I. G. Ivanov, B. Magnusson, and N. T. Son, in *Defects in Microelectronic Materials and Devices*, edited by D. Fleetwood and R. Schrimpf (Taylor & Francis, 2008), pp. 615–670.

[38]L. W. Aukerman and M. F. Millea, Phys. Rev. **148**, 759 (1966).

[39]W. Suttrop, G. Pensl, and P. Lanig, Appl. Phys. A **51**, 231 (1990).

[40]W. Lambrecht, S. Limpijumnong, S. Rashkeev, and B. Segall, Phys. Status Solidi B **202**, 5 (1997).

[41]W. Suttrop, G. Pensl, W. J. Choyke, R. Stein, and S. Leibenzeder, J. Appl. Phys. **72**, 3708 (1992).

[42]A. Koizumi, V. P. Markevich, N. Iwamoto, S. Sasaki, T. Ohshima, K. Kojima, T. Kimoto, K. Uchida, S. Nozaki, B. Hamilton, and A. R. Peaker, Appl. Phys. Lett. **102**, 032104 (2013).

[43]M. Lax, Phys. Rev. **119**, 1502 (1960).

[44]V. Abakumov, V. Perel, and I. Yassievich, Sov. Phys. Semicond. **12**, 1 (1978).

[45]P. B. Klein, B. V. Shanabrook, S. W. Huh, A. Y. Polyakov, M. Skowronski, J. J. Sumakeris, and M. J. O'Loughlin, Appl. Phys. Lett. **88**, 052110 (2006).

[46]Here we have implemented different values of k for $\sigma_{i,h} = k \times \sigma_{i,e}^{+/0}$. in the negative-$U$ centers related carrier dynamics simulations where $k \in [5, 10]$. It was found that the variation of k within such a range does not affect the simulated TRPL decay curve.

[47]L. F. Shampine and M. W. Reichelt, SIAM J. Sci. Comput. **18**, 1 (1997).

[48]W. Shockley and J. T. Last, Phys. Rev. **107**, 392 (1957).

[49]A. A. Lebedev, Semiconductors **33**, 107 (1999).

[50]K. Neimontas, T. Malinauskas, R. Aleksiejūnas, M. Sūdžius, K. Jarašiūnas, L. Storasta, J. P. Bergman, and E. Janzen, Semicond. Sci. Technol. **21**, 952 (2006).

[51]N. Ramungul, V. Khemka, T. Chow, M. Ghezzo, and J. W. Kretchmer, Mater. Sci. Forum **264–268**, 1065 (1998).

[52]A. Galeckas, J. Linnros, V. Grivickas, U. Lindefelt, and C. Hallin, Appl. Phys. Lett. **71**, 3269 (1997).

[53]A. B. Sproul, J. Appl. Phys. **76**, 2851 (1994).

[54]A. Galeckas, J. Linnros, M. Frischholz, K. Rottner, N. Nordell, S. Karlsson, and V. Grivickas, Mater. Sci. Eng. B **61–62**, 239 (1999).

[55]M. Ikeda, H. Matsunami, and T. Tanaka, Phys. Rev. B **22**, 2842 (1980).

[56]K. Gulbinas, P. Ščajev, V. Bikbajavas, V. Grivickas, O. V. Korolik, A. V. Mazanik, A. K. Fedotov, V. Jokubavičius, M. K. Linnarsson, M. Syväjärvi, and S. Kamiyama, IOP Conf. Ser.: Mater. Sci. Eng. **56**, 012005 (2014).

[57]P. Ščajev and K. Jarašiunas, J. Phys. D **46**, 265304 (2013).

[58]V. Grivickas, K. Gulbinas, V. Jokubaviius, J. W. Sun, M. Karalinas, S. Kamiyama, M. Linnarsson, M. Kaiser, P. Wellmann, and M. Syväjärvi, IOP Conf. Ser.: Mater. Sci. Eng. **56**, 012004 (2014).

[59]S. A. Reshanov, K. Schneider, R. Helbig, G. Pensl, H. Nagasawa, and A. Schöner, Mater. Sci. Forum **457–460**, 513 (2004).

[60]K. Danno, D. Nakamura, and T. Kimoto, Appl. Phys. Lett. **90**, 202109 (2007).

[61]A. Suzuki, H. Matsunam, and T. Tanaka, J. Phys. Chem. Solids **38**, 693 (1977).

[62]S. Hagen, A. Van Kemenade, and J. Van Der Does De Bye, J. Lumin. **8**, 18 (1973).

[63]I. Pintilie, L. Pintilie, K. Irmscher, and B. Thomas, Appl. Phys. Lett. **81**, 4841 (2002).

[64]V. Jokubavicius, M. Kaiser, P. Hens, P. J. Wellmann, R. Liljedahl, R. Yakimova, and M. Syväjärvi, Mater. Sci. Forum **740–742**, 19 (2013).

[65]T. Kimoto, K. Hashimoto, and H. Matsunami, Jpn. J. Appl. Phys., Part 1 **42**, 7294 (2003).

[66]C. Wang, J. Bernholc, and R. F. Davis, Phys. Rev. B **38**, 12752 (1988).

[67]H. Itoh, A. Kawasuso, T. Ohshima, M. Yoshikawa, I. Nashiyama, S. Tanigawa, S. Misawa, H. Okumura, and S. Yoshida, Phys. Status Solidi A **162**, 173 (1997).

[68]M. Yamanaka, H. Daimon, E. Sakuma, S. Misawa, and S. Yoshida, J. Appl. Phys. **61**, 599 (1987).

[69]H. J. Kim and R. F. Davis, J. Electrochem. Soc. **133**, 2350 (1986).

[70]W. Shockley and W. T. Read, Phys. Rev. **87**, 835 (1952).

[71]D. G. Thomas, J. J. Hopfield, and W. M. Augustyniak, Phys. Rev. **140**, A202 (1965).

[72]T. Kimoto and J. A. Cooper, *Fundamentals of Silicon Carbide Technology* (John Wiley & Sons Singapore Pte. Ltd, 2014), pp. 11–38.

[73]G. Harris, *Properties of Silicon Carbide*, EMIS Data Reviews Series (INSPEC, the Institution of Electrical Engineers, 1995).

[74]C. Persson, U. Lindefelt, and B. E. Sernelius, J. Appl. Phys. **86**, 4419 (1999).

[75]Y. Varshni, Physica **34**, 149 (1967).